THE JOURNAL OF PHYSICAL CHEMISTRY C

Article

pubs.acs.org/JPCC

Dealloying of Cobalt from CuCo Nanoparticles under Syngas Exposure

Sophie Carenco,[†] Anders Tuxen,[†] Mahati Chintapalli,[†,‡] Elzbieta Pach,[†] Carlos Escudero,[†] Trevor D. Ewers,[†,§] Peng Jiang,[†] Ferenc Borondics,[†] Geoff Thornton,[†,∥] A. Paul Alivisatos,[†,§] Hendrik Bluhm,[#] Jinghua Guo,[⊥] and Miquel Salmeron*[,†,‡]

[†]Materials Sciences Division, [⊥]Advanced Light Source, and [#]Chemical Sciences Division, Lawrence Berkeley National Lab, Berkeley, California 94720, United States

[‡]Department of Materials Sciences and [§]Department of Chemistry, University of California Berkeley, Berkeley, California 94720, United States

[∥]London Centre for Nanotechnology and Chemistry Department, University College London, 20 Gordon Street, London WC1H 0AJ, United Kingdom

Supporting Information

ABSTRACT: The structure and composition of core−shell CuCo nanoparticles were found to change as a result of cleaning pretreatments and when exposed to syngas (CO + H_2) at atmospheric pressure. In situ X-ray absorption and photoelectron spectroscopies revealed the oxidation state of the particles as well as the presence of adsorbates under syngas. Transmission electron microscopy was used for ex situ analysis of the shape, elemental composition, and structure after reaction. The original core−shell structure was found to change to a hollow CuCo alloy after pretreatment by oxidation in pure O_2 and reduction in pure H_2. After 30 min of exposure to syngas, a significant fraction (5%) of the particles was strongly depleted in cobalt giving copper-rich nanoparticles. This fraction increased with duration of syngas exposure, a phenomenon that did not occur under pure CO or pure H_2. This study suggests that Co and Cu can each individually contribute to syngas conversion with CuCo catalysts.

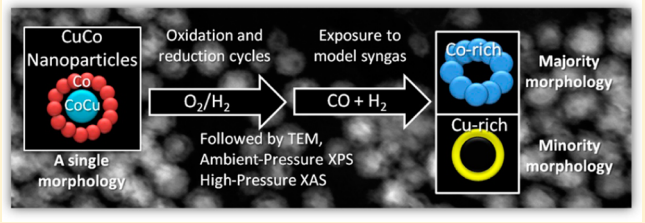

1. INTRODUCTION

Environmental concerns have sparked renewed interest in the Fischer−Tropsch process to synthesize clean fuels from syngas (CO + H_2), which can be produced from abundant raw materials such as coal or biomass. Although the activity and selectivity of this process have been improved over several decades,[1,2] fundamental issues about the reaction mechanism and the structure of the catalyst remain unsolved.[3] While catalyst turnover frequency (reactivity) is an important characteristic, selectivity is the most desirable property. With the development of modern methods of nanoparticle (NP) synthesis with controlled size, shape, and composition, the goal of high selectivity can be achieved. Equally important to the synthesis of catalysts, new in situ microscopy and spectroscopy tools are needed to understand the reaction mechanisms to inform catalyst design and improve reaction efficiency.

Among the surface-sensitive techniques, synchrotron-based core level spectroscopies such as X-ray photoelectron spectroscopy (XPS) and soft X-ray absorption spectroscopy (XAS) are among the most well-suited to investigate the state of the catalyst. Recent developments in instrumentation allow spectra to be collected in the presence of gaseous environments that mimic the operating conditions of industrial catalytic systems, although the typical pressures for Fischer−Tropsch synthesis are higher (ca. 20 bar).[4] These techniques include ambient-pressure XPS (AP-XPS, up to several torr of gas)[5] and high-pressure XAS (HP-XAS, up to 1−5 bar).[6−10]

In the case of Fischer−Tropsch synthesis, pure cobalt catalysts provide a high yield of paraffins and olefins and a poor yield of oxygenated products, due to the high dissociation rate of CO.[11] Particle size effects have been extensively studied in cobalt NPs with the goal of tuning their activity and selectivity.[12−15] Bimetallic catalysts open additional avenues for improving selectivity.[16,17] It has been shown, for example, that adding copper to cobalt catalysts prepared by impregnation−reduction promotes the formation of oxygenated products.[18]

Although it is well established that bulk CuCo alloys do not exist due to the low solubility of one metal into the other,[19] recent studies suggest that such alloys may form at the nanoscale.[20,21] Nanoscale alloying of Co and Cu could be responsible for the peculiar selectivity of Co/Cu catalysts,[21] since a mechanical mixture of both metals does not change the cobalt's selectivity.[22] Selectivity for short-chain alcohol

Received: January 2, 2013
Revised: March 4, 2013
Published: March 5, 2013

production was demonstrated by Subramanian et al.[23] using core−shell Cu−Co_3O_4 NPs. Using in situ diffuse reflectance IR Fourier transform spectroscopy (DRIFTS), the authors illustrated the competition between dissociative and molecular adsorption of CO on the NPs. However, the nanoscale evolution of the catalyst during the reaction is still poorly understood.

To better understand the nanoscale evolution of the catalyst, we prepared well-defined CuCo core−shell NPs and followed their morphology and chemical composition during pretreatment (reduction and oxidation cycles) and under catalytic conditions (exposure to a model CO/H_2 syngas mixture). A combination of characterization techniques was employed, including in situ spectroscopies (AP-XPS and HP-XAS) and ex situ transmission electron microscopy (TEM).

2. RESULTS

2.1. Morphological Structure Following Pretreatment and Exposure to Syngas. CuCo composite NPs of diameter 22 ± 4 nm and with a Cu/Co ratio of 1:9 (±10%), as verified by X-ray energy dispersive analysis, were prepared according to literature procedures (see the Supporting Information) and drop cast onto Si_3N_4 membrane TEM grids for analysis.[24] The as-prepared NPs exhibited a core−shell morphology with a copper−cobalt core and a cobalt shell (Figure 1). They were all

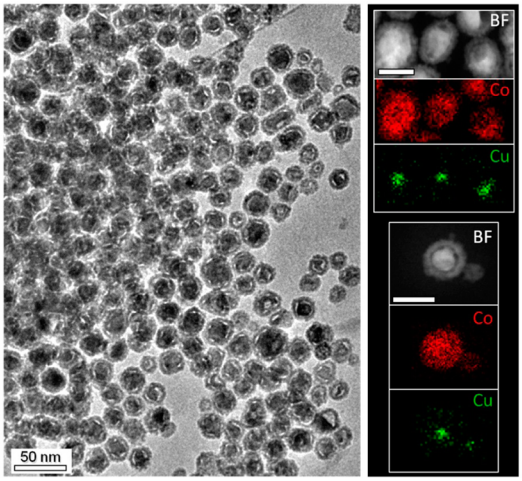

Figure 1. (left) Bright-field TEM image of the as-prepared core−shell NPs. (right) STEM-EDS chemical analysis of the nanoparticles. The overall Cu/Co ratio is 1:9.

of the same composition to within 10%, and in particular, no copper-rich NPs were observed at this stage in over a thousand NPs analyzed at different points on the TEM grid. The NPs deposited on the TEM grid were then pretreated in a quartz tube reactor to remove surfactants used in the synthesis, thus lowering the amount of carbon and oxygen on their surface. The pretreatment, similar to those typically applied to other heterogeneous catalysts, consisted of cycles of oxidation at 200 °C for 15 min under O_2 (1 atm) and reduction at 250 °C for 15 min under H_2 (1 atm). Examination of the pretreated NPs by TEM revealed that the original core−shell structure, with a CuCo core and a Co shell, had transformed into a hollow structure with the shell consisting of a CuCo alloy (Supporting Information, Figure 1). No change of composition was observed at this stage, and the NPs exhibited as before a Cu/Co ratio of 1:9 (±10%).

To examine the next stage in the process, syngas exposure, fresh NPs were drop-cast onto a TEM grid, pretreated by oxidation and reduction, and finally, exposed to model syngas (CO/H_2 = 1:3) at 250 °C at 1 atm for 30 min. After reaction, the NPs were transferred through air to the TEM. The resulting images are shown in Figure 2. While the hollow CuCo

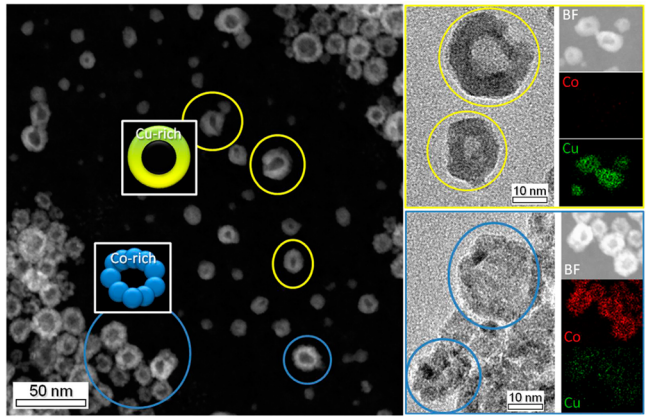

Figure 2. (left) High angle annular dark field image of the NPs after pretreatment and exposure to syngas, showing two new morphologies: hollow Co-rich NPs with a Cu/Co ratio of 1:9 (blue-circled) and smooth hollow Cu-rich NPs with a Cu/Co ratio of 9.5:0.5 (yellow-circled). (right) Bright-field TEM and STEM-EDS images of the two NP morphologies observed after exposure to syngas (Cu-rich on top, Co-rich on the bottom).

polycrystalline alloy shell structure that formed during pretreatment was preserved in about 95% of the NPs (marked by blue circles in the figure), scanning TEM with energy dispersive X-ray spectroscopy (STEM-EDS) revealed that significant changes in particle composition occurred in the remaining 5% of the NPs. These NPs exhibited smooth shell morphologies and were highly depleted in cobalt, with Cu/Co ratios of 9.5:0.5 as revealed by EDS. They were homogeneously dispersed on the whole membrane and were easily detected by performing the chemical mapping on a region containing hundreds of NPs. The high-resolution TEM (HRTEM) images of these copper-rich NPs (Supporting Information, Figure 2) show a polycrystalline structure with lattice parameters compatible with those of Cu_4O_3, while the images of the majority Co-rich NPs showed a highly polycrystalline mixed $Co_xCu_yO_4$ oxide (Supporting Information, Figure 3), with a Cu/Co ratio of 1:9, as in the initial NPs. An important finding is that no Cu-rich NPs were formed when exposing the sample to CO only, verified by examining more than a thousand NPs (see for instance Supporting Information, Figure 4).

2.2. In Situ Spectroscopy Studies. To gain insight into the processes leading to the formation of hollow alloy NPs and the reversal of the Cu/Co stoichiometry under syngas, in situ AP-XPS and HP-XAS experiments were conducted at beamlines 11.0.2 and 7.0.1 of the Advanced Light Source at Lawrence Berkeley National Laboratory. While spectroscopy was not expected to provide a direct measurement of the stoichiometry evolution affecting some of the NPs, it proved successful to identify relevant differences in the surface state of particles exposed to various gas atmospheres (H_2, CO, or both H_2 and CO).

First, both the XPS and XAS data show that, after the pretreatment (oxidation−reduction cycles), the NPs are in a

dx.doi.org/10.1021/jp4000297 | J. Phys. Chem. C 2013, 117, 6259−6266

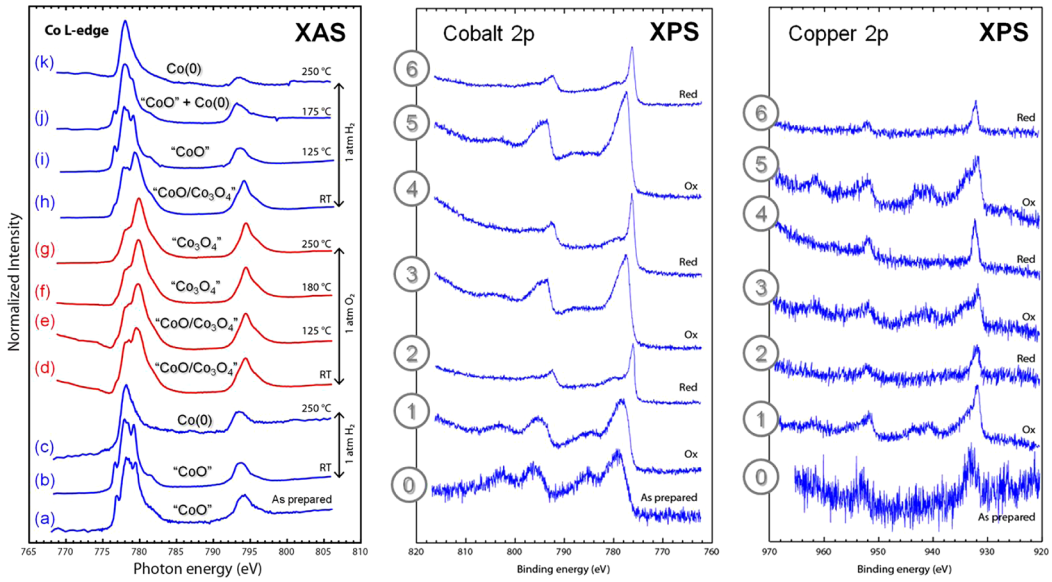

Figure 3. (left) HP-XAS analysis of the NPs after oxidation and reduction under 1 atm of O_2 or H_2. (a–k) Spectra were recorded under vacuum after exposure to gas (H_2 for b and c and h–k; O_2 for d–g) at the temperatures indicated. (right) AP-XPS spectra showing oxidation–reduction cycles of the NPs. "Ox" spectra were acquired after exposure to 1 Torr of O_2 at 250 °C and "Red" spectra were acquired after exposure to 5 Torr of H_2 at 330 °C. Spectrum 0 corresponds to the nanoparticles as prepared, and spectra 1–6 correspond to successive oxidation (odd numbers) and reduction (even numbers). The spectra labeled 0–6 correspond to those in Figure 4.

metallic state (Figure 3). In the HP-XAS gas cell, where the pressure could be raised to 1 atm,[10] the spectra (Figure 3, left) were recorded using the total electron yield (TEY) current collected at a gold foil supporting the NPs. Using the TEY makes the technique surface-sensitive (electron mean free path is approximately 2 nm). Heating to 250 °C under 1 atm of H_2 fully reduced the NPs (spectra c and k). After exposure to 1 atm of O_2, a mixed oxide containing Co(II) and Co(III) (spectrum d) was observed at room temperature, referred to as "CoO/Co_3O_4" because of its similarity to the spectrum of a copper-free $Co^{(II)}O$ and $Co^{(II,III)}{}_3O_4$ mixture.[25,8,26] Further heating in O_2 to 180 °C converted the CoO to Co_3O_4 (spectrum f). The NPs could be reduced back to metallic cobalt (spectrum k) through the same intermediate states: CoO/Co_3O_4 mixture, CoO, and CoO/Co(0) by heating in 1 atm of H_2.

In the AP-XPS chamber, where the pressure is limited to a few torr, a higher temperature was needed to fully reduce the NPs. As shown by the XPS spectra in Figure 3, the NPs could be reversibly reduced to the metallic state under 5 Torr of H_2 at 330 °C. On the basis of comparison with pure cobalt NPs,[27] we note that the presence of copper facilitates the reduction of the NPs at a lower temperature, in agreement with previous studies on CoCu[28] and FeCu[29] NPs prepared by coimpregnation of salts.

We also investigated the surface composition of the NPs in successive oxidation and reduction cycles using photoelectrons of low kinetic energy (200 eV), which have a short mean free path. The atomic fractions derived from the areas of the Cu and Co XPS peaks are shown in Figure 4. A small but clear cobalt enrichment of the surface was observed under reducing conditions, which indicates that, even at pressures in the torr range, structural changes occur. Hence, AP-XPS can give insight into the chemical changes that may play a role in the Cu–Co segregation under atmospheric conditions.

In order to elucidate the role of the gas environment on Cu and Co segregation, AP-XPS was used to in situ study the

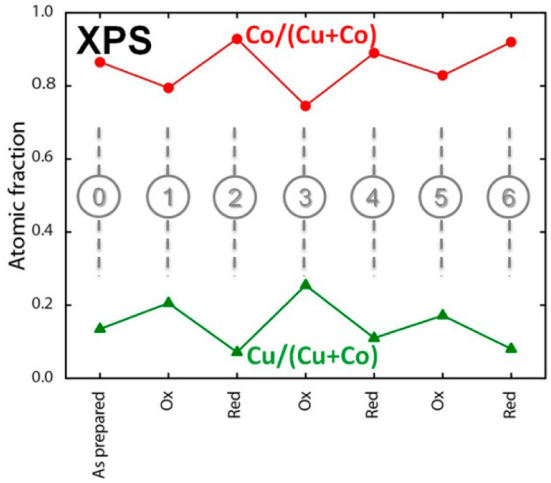

Figure 4. AP-XPS analysis of the surface composition of the NPs after oxidation (1 Torr of O_2) and reduction (5 Torr of H_2). The numbers 0–6 correspond to the XPS spectra in Figure 3.

surface composition of the NPs, with pressure in the torr range in this case. The spectra in Figure 5 show the O1s peak spectral region after reduction (A), in 200 mTorr of CO (B), and in a syngas mixture of 200 mTorr of CO and 200 mTorr of H_2 (C).[30] The corresponding C1s spectra are plotted in Figure 5 of the Supporting Information.

After the reduction step, two C peaks, at 284.0 eV (C4) and 285.8 eV (C3), and two oxygen peaks, at 529.6 eV (O3) and 531.5 eV (O2), are observed (Figure 5 and the Supporting Information, Figure 5). The small peak at 529.6 eV corresponds to residual CoO_x. The 285.8 eV (C3) and the 531.5 eV (O2) peaks can be assigned to C and O from adsorbed CO molecules by comparison with the relative areas and the position of the peaks from CO adsorbed on a Co foil (not shown here). A contribution from residual OH species to the 531.5 eV peak is possible as well. Carbide, graphite, and CH_x species all have

dx.doi.org/10.1021/jp4000297 | J. Phys. Chem. C 2013, 117, 6259–6266

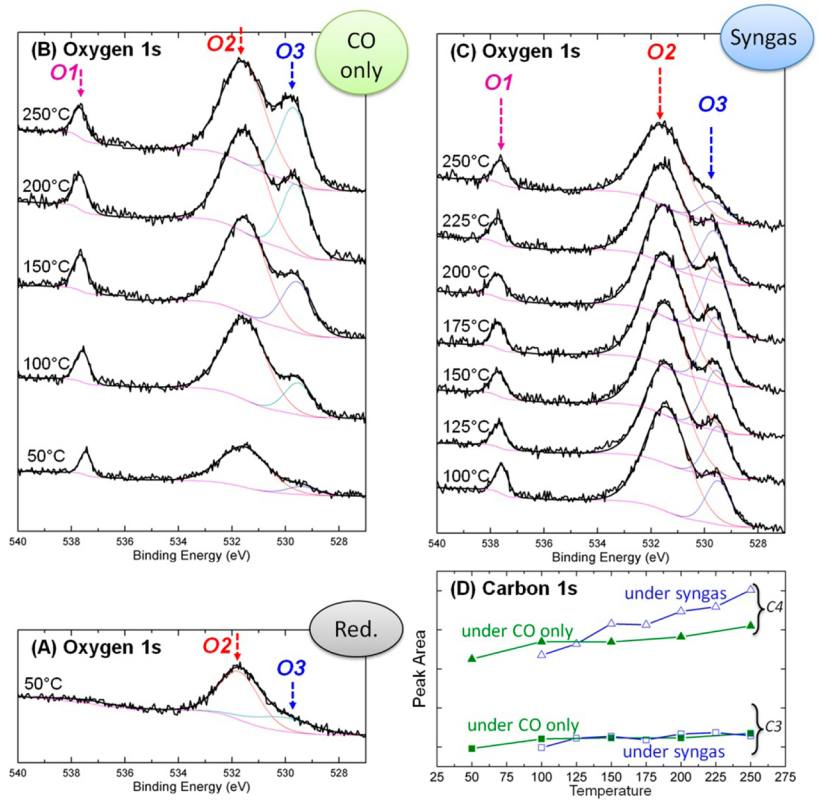

Figure 5. (A–C) AP-XPS O1s spectra of pretreated reduced NPs (spectrum A) while exposed to CO (200 mTorr, spectra B) or syngas (CO 200 mTorr and H_2 200 mTorr, spectra C), upon heating (temperatures are indicated on the spectra). (D) Peak area obtained from the C1s spectra (plotted on Figure 5 of the Supporting Information) for peak C4 at 284 eV (triangles) and C3 at 285.8 eV (squares) under syngas (blue hollow symbols) or CO only (green plain symbols).

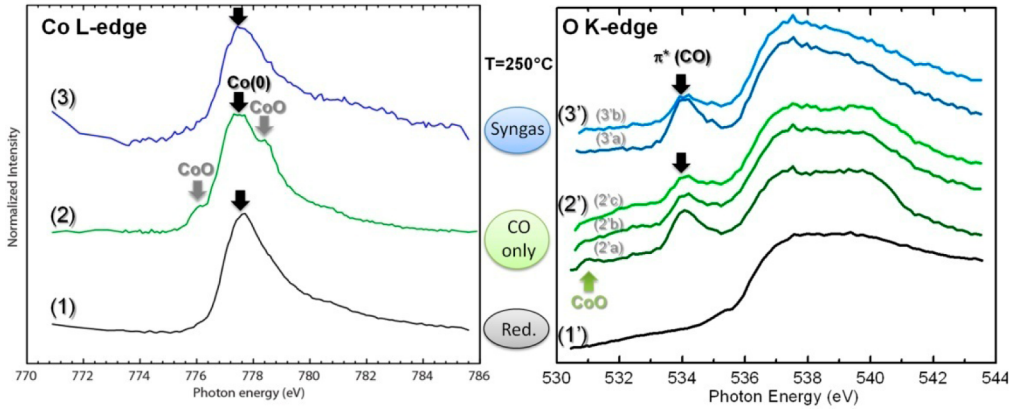

Figure 6. In situ HP-XAS Co *L*-edge (left) and O *K*-edge (right) spectra of pretreated reduced NPs (spectra 1 and 1′) exposed to CO (1 atm, spectra 2 and 2′) or syngas (1 atm, CO/H_2 in a 1:3 ratio, spectra 3 and 3′) at 250 °C. Spectra were recorded under helium (1 atm).

peaks in the 284 eV region (C4) and are likely to be present on the surface as contaminants, although we did not attempt to deconvolute the peak into more than one component. The presence of CO on the NP surface after pumping out H_2 following the final reduction step is due to residual background CO gas (10^{-6} to 10^{-7} Torr) and the high reactivity of clean Co.[27] Although DRIFTS experiments by Smith et al. suggested that CO preferentially adsorbs on Cu at low temperature and on Co at higher temperature (>200 °C),[31] we could not determine its adsorption site, since the C1s peaks from CO have similar binding energies on each metal (respectively, 285.6 and 285.4 eV), as verified using a Co foil and a Cu foil for reference (not shown here).

Upon introduction of 200 mTorr of CO, the C3 (285.8 eV) and O2 (531.5 eV) peaks remain mostly unchanged, indicating that the NPs surface was saturated by CO. Peaks due to gas-phase CO are observed at higher binding energies of 537.6 eV (O1) and 291.4 eV (C1) for O and C, respectively. As the temperature increased, the oxide peak at 529.6 eV (O3) and the C peak at 284 eV (C4, see Figure 5D) increased, indicating decomposition of the CO. The areas of the molecular CO peaks at 531.5 (O2) and 285.8 eV (C3, peak area plotted in Figure 5D) remain unchanged, which indicates that the gas-

dx.doi.org/10.1021/jp4000297 | J. Phys. Chem. C 2013, 117, 6259–6266

phase CO replenishes the molecules lost due to dissociation. Although no hydrogen was introduced into the chamber, in our previous work on pure Co NPs,[27] we showed that H is necessary for the efficient dissociation of CO and that even small amounts of H are sufficient for that purpose. We believe that the presence of small amounts of H_2 is practically unavoidable in the background gas.

The sample was cleaned again with an oxidation−reduction cycle (Figure 5A), and a syngas mixture consisting of 200 mTorr of H_2 and 200 mTorr of CO was introduced in the chamber (Figure 5C). The spectra at 100 °C show both molecular CO (peaks O2 and C3 at 531.5 and 285.8 eV, respectively) and oxide and carbide peaks at 529.6 eV (O3) and 284 eV (C4). The oxide peak is now more intense due to the dissociation of CO aided by the hydrogen.[27] As the temperature increases, no changes are observed until 250 °C, at which point a rapid decrease of the oxide peak is clearly visible, as shown in the top spectra of Figure 5C. In pure H_2 gas, the two peaks oxide (O3) and CO (O2) decrease due to reaction with H to dissociate CO and to make H_2O and CH_x species. The formation of these latter species is confirmed by the increase of the area of peak C4 at 284 eV, as observed in Figure 5D (empty triangles).

In situ HP-XAS (Figure 6) confirmed these findings. The pretreated reduced NPs exposed to 1 atm of CO were found to be partially oxidized, as shown by the Co *L*-edge spectrum that is a mixture of Co(0) and CoO, while they were fully reduced before CO was added (Figure 6, spectrum 1). The situation was different after exposure to syngas (1 atm of CO/H_2 in a 1:3 ratio) at 250 °C where the cobalt was found to be in the reduced state (spectrum 3), in agreement with the AP-XPS observations. The presence of molecular CO on the surface gives rise to the absorption peak at 534 eV, corresponding to the O1s → $2\pi^*$ orbital transition.[32] The intensity of this peak decreased with time within minutes (spectra 2′b and 3′b collected after 5 min and 2′c after 10 min), indicating that CO does not stay molecularly adsorbed on the surface at 250 °C due to dissociation and reaction to produce H_2O and CH_x. The broad signal from 536 to 542 eV, present in all the conditions investigated, is reminiscent of adsorbed molecular water[33] and hydroxyl species, in agreement with the AP-XPS observations and the DRIFTS observations.[14]

2.3. Mechanism of Co−Cu Segregation. As shown in the first section of the paper, dealloying of cobalt nanoparticles out of CuCo was observed experimentally for 5% NPs. The copper-rich particles were hollow with shell of irregular thickness, and they had an outer diameter between 10 and 20 nm. It is assumed that their diameter and/or shell thickness were reduced compared to those of the parent particles, since matter was extracted out of them. However, size comparison is hardly possible using ex situ TEM because of the intrinsic size distribution of the nanoparticles (some of them have diameter significantly larger than the average 22 nm) and because they are analyzed after exposure to air during transfer to the microscope, which also affects their volume because of oxidation. This point will be investigated in further details using in situ TEM and looking for size evolution of a given nanoparticle in a dedicated study.

Altogether, the results in the previous sections allow us to propose a mechanism to explain the segregation of Co from the Cu-rich NP to form nearly pure Cu NPs.

As mentioned above, the Cu enrichment of NPs only takes place under exposure to syngas while pure CO is not effective. This is because CO dissociates (with the help of small amounts of H), to produce cobalt oxides, which do not react to form carbonyls. In the presence of syngas, with abundant H_2 in the gas phase, the NPs maintain their metallic state because H_2 continually removes both C (from CO dissociation) by converting it to CH_4, and Co oxide, by reacting with it to form water.

The formation of Cu-rich NPs could be the result of Cu atom diffusion, and nucleation on new sites on the surface does not seem to be the relevant mechanism in the particular set of conditions of our study (<250 °C, low starting Cu/Co ratio). Other works have identified the mobility of copper on oxide surfaces at elevated temperature (ca. 300 °C) under H_2 exposure.[34] But, the facts that (i) the hollow morphology is preserved, (ii) no very small or very large Cu nanoparticles was observed (as it would be the case if a new process of nucleation was involved), and (iii) this process is observed here only under the synergetic effect of CO and H_2 argue strongly against the mechanism of copper migration in this particular case.

In contrast with this, the enhanced migration of metallic atoms under exposure to low pressure of CO (up to 10 mbar) was recently observed in the case of platinum NPs, which do not form an oxide under these conditions.[35] In the present case, the reductive H_2 environment is essential as it keeps the cobalt surface active and metallic so that CO can still bind strongly to it. The formation of copper-rich NPs appears as a CO-induced phenomenon.

We propose that the CO-induced copper enrichment by cobalt extraction, which preserves the hollow morphology of the particles, is due to the formation of cobalt carbonyl species from the reduced NPs. CO binds relatively weakly to the copper surface (11−14 kcal/mol),[36] while it binds more strongly to cobalt surfaces such as Co(110) (ca. 33 kcal/mol).[37] Smith et al. have noted that, on mixed CoCu catalysts, CO binds even more strongly than on pure cobalt catalysts.[31] It is thus not easy to predict the heat of adsorption on the present NPs, but in any case, a strong adsorption on Co sites can be expected. Formation of Cu−carbonyls is very unlikely, as density functional theory calculations suggest a very weak Cu−CO bond (6 kcal/mol),[38] while Co−carbonyls (such as $Co_2(CO)_8$, $HCo(CO)_4$, or $Co_4(CO)_{12}$) are stable.

Two scenarios are possible to explain the CO-induced dealloying. One is gas-phase transfer because $Co_2(CO)_8$ is known to form in equilibrium with a cobalt metal surface at 150 °C under 40 bar (with a heat of formation of 55 kcal/mol).[39] The pressure is lower here, but the higher temperature and the continuous flow of syngas could act as driving forces,[40] as the carbonyl can sublime easily once formed (sublimation enthalpy for $Co_2(CO)_8$ is 15.6 kcal/mol).[41,42] In the second scenario, Co−carbonyl species could form and migrate on the surface, redepositing on some of the cobalt-rich NPs. Detailed studies involving the influence of the support should be conducted in the future to discriminate between the two possibilities.

Lastly, it should be noted that only two extreme compositions were observed (Co-rich and Cu-rich), suggesting that the extraction of cobalt from some of the NPs is a self-enhanced process, with a high activation energy barrier but no further kinetic limitation: once started, it goes rapidly to its end. This could be facilitated by the surface enrichment in cobalt observed under reducing conditions. Apparently, the intermediate compositions that are alloys of Co and Cu do not seem to be stable under these conditions. It should be noted that this process was rather limited, affecting 5% of the NPs within the

dx.doi.org/10.1021/jp4000297 | J. Phys. Chem. C 2013, 117, 6259−6266

relatively short exposure time reported here (30 min). A longer exposure time of 2 h increased this population to 15%. Our mechanistic hypothesis could be tested in further work by using environmental TEM equipped with a gas cell to study this phenomenon in situ. Such studies are planned in the near future, as they could also give insights into the structural reasons favoring the dealloying in some particles over others. Scheme 1 summarizes all these observations graphically.

Scheme 1. Step-by-Step in Situ and ex Situ Observations of the Behavior of CuCo NPs

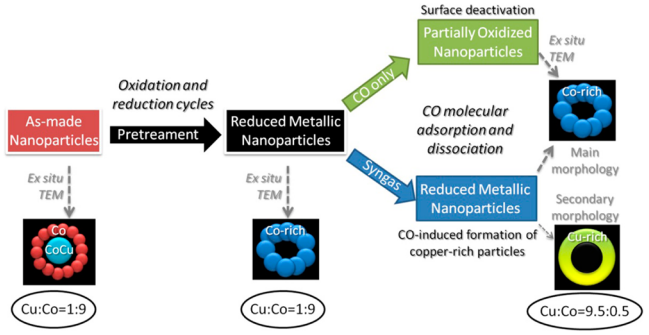

In conclusion, while most studies dealing with CuCo catalysts emphasize the synergistic effect of the two metals in the alloy on catalyst selectivity, the segregation of copper and cobalt found in our experiments brings a new element that should be taken into consideration in the actual operation of the catalyst and into the design of new structures. The understanding of how the final structure and composition is determined by the operating conditions of the catalyst could then guide new designs to achieve a configuration with optimal selectivity. In situ studies, currently done with AP-XPS and HP-XAS show the way to understand these phenomena. Experiments with in situ TEM are also very important and will be pursued in the near future.

3. EXPERIMENTAL SECTION

(i) Chemical state of the surface of the nanoparticles was analyzed in situ by AP-XPS, which allows exposure of the NPs to gas up to a few torr. The experiments were conducted at beamline 11.0.2 of the Advanced Light Source in Berkeley, California. A monolayer of NPs was deposited on a gold foil using the Langmuir–Blodgett technique. The gold foil was used as an inert supporting substrate for the NPs, and its Au4f and Au4d peaks were used to calibrate the binding energies of O1s and C1s peaks and to normalize the spectra. O1s and C1s peaks were measured with a photon energy of 700 eV. Co2p peaks were measured with a photon energy of 980 eV, and Cu2p peaks were measured with an energy of 1140 eV.

(ii) The oxidation state of the particles was followed in situ using HP-XAS, under chosen gas mixture exposure at atmospheric pressure: O_2, H_2, CO, CO/H_2 (1:3 ratio), diluted two times in He. These experiments were conducted at beamline 7.0.1 of the Advanced Light Source in Berkeley, California. For the XAS experiments, the NPs were deposited on a gold foil. The foil was then introduced in a newly designed gas cell equipped with a laser heating stage, so that the high-pressure region is confined to the inside of the cell.[10] XAS spectra were recorded using the TEY mode on both the Co *L*-edge and the O *K*-edge.

(iii) Chemical analysis and HRTEM of the NPs was done ex situ using a JEOL 2100F TEM operated at 200 kV either in HRTEM mode or in STEM mode with a probe size of 1 nm for high angle annular dark field and EDS-mapping analyses. The NPs were deposited from a diluted solution in hexanes by drop-casting on a Si_3N_4 grid. In order to investigate the evolution of their morphology under gas exposure, the CuCo NPs were deposited on a Si_3N_4 TEM grid (considered an inert substrate) and then treated using a homemade U-shape quartz reactor. The reactor was operated at atmospheric pressure, and mass flow controllers at the inlet were used to regulate the gas composition. The NPs were oxidized under O_2/He at 200 °C and reduced under H_2 at 250 °C, in order to simulate the catalyst pretreatment. It should be noted that the NPs were exposed to air at room temperature during the transfer of the grid from the reactor to the TEM.

(iv) The NPs were prepared according to a previously described thermal decomposition route and according to ref 24 (see the Supporting Information).

■ ASSOCIATED CONTENT

Ⓢ Supporting Information

Experimental procedures and additional TEM, HRTEM, EDS, and AP-XPS data. This material is available free of charge via the Internet at http://pubs.acs.org.

■ AUTHOR INFORMATION

Corresponding Author

*Phone: (510) 486-6704; e-mail: mbsalmeron@lbl.gov.

Notes

The authors declare no competing financial interest.

■ ACKNOWLEDGMENTS

This work was supported by the Director, Office of Science, Office of Basic Energy Sciences, Chemical Sciences, Geosciences, and Biosciences Division, under the Department of Energy contract no. DE-AC02-05CH11231. Funding from the same contract for the ALS and beamline 11.0.2 is also acknowledged. The Molecular Foundry is acknowledged for the use of its facilities under the proposal no. 994. Virginia Altoe is gratefully acknowledged for helpful discussions concerning TEM analyses. A.T. gratefully acknowledges the postdoc stipend "In-situ investigations of nanoparticles for Fischer–Tropsch catalysis" from the Danish Research Council for Independent Research | Natural Sciences (Det Frie Forskningsraad | Natur og Univers). C.E. acknowledges financial support from the MEC/Fulbright program (reference no. 2008-0253). G.T. acknowledges support from EPSRC (UK).

■ REFERENCES

(1) Schulz, H. Short History and Present Trends of Fischer–Tropsch Synthesis. *Appl. Catal., A* **1999**, *186*, 3–12.

(2) (a) Dry, M. E. High Quality Diesel via the Fischer–Tropsch Process – A Review. *J. Chem. Technol. Biotechnol.* **2002**, *77*, 43–50. (b) Dry, M. E. The Fischer–Tropsch Process: 1950–2000. *Catal. Today* **2002**, *71*, 227–241.

(3) (a) Rofer-DePoorter, C. K. A Comprehensive Mechanism for the Fischer−Tropsch Synthesis. *Chem. Rev.* **1981**, *81*, 447−474. (b) Van Der Laan, G. P.; Beeneckers, A. A. C. M. Kinetics and Selectivity of the Fischer−Tropsch Synthesis: A Literature Review. *Catal. Rev.* **1999**, *41*, 255−318. (c) Davis, B. H. Fischer−Tropsch Synthesis: Current Mechanism and Futuristic Needs. *Fuel Process. Technol.* **2001**, *71*, 157−166. (d) Cheng, J.; Gong, X.; Hu, P.; Lok, C.; Ellis, P.; French, S. A Quantitative Determination of Reaction Mechanisms from Density Functional Theory Calculations: Fischer−Tropsch Synthesis on Flat and Stepped Cobalt Surfaces. *J. Catal.* **2008**, *254*, 285−295. (e) Ojeda, M.; Nabar, R.; Nilekar, A. U.; Ishikawa, A.; Mavrikakis, M.; Iglesia, E. CO Activation Pathways and the Mechanism of Fischer−Tropsch Synthesis. *J. Catal.* **2010**, *272*, 287−297.

(4) Escudero, C.; Salmeron, M. From Solid−Vacuum to Solid−Gas and Solid−Liquid Interfaces: In Situ Studies of Structure and Dynamics under Relevant Conditions. *Surf. Sci.* **2013**, *607*, 2−9.

(5) Ogletree, D. F.; Bluhm, H.; Lebedev, G.; Fadley, C. S.; Hussain, Z.; Salmeron, M. A Differentially Pumped Electrostatic Lens System for Photoemission Studies in the Millibar Range. *Rev. Sci. Instrum.* **2002**, *73*, 3872.

(6) Knop-Gericke, A.; Hävecker, M.; Schedel-Niedrig, T.; Schlögl, R. High-Pressure Low-Energy XAS: A New Tool for Probing Reacting Surfaces of Heterogeneous Catalysts. *Top. Catal.* **2000**, *10*, 187−198.

(7) Salmeron, M.; Schlögl, R. Ambient Pressure Photoelectron Spectroscopy: A New Tool for Surface Science and Nanotechnology. *Surf. Sci. Rep.* **2008**, *63*, 169−199.

(8) Bazin, D.; Guczi, L. Soft X-Ray Absorption Spectroscopy in Heterogeneous Catalysis. *Appl. Catal., A* **2001**, *213*, 147−162.

(9) Bare, S. R.; Yang, N.; Kelly, S. D.; Mickelson, G. E.; Modica, F. S. Design and Operation of a High Pressure Reaction Cell for in Situ X-Ray Absorption Spectroscopy. *Catal. Today* **2007**, *126*, 18−26.

(10) Escudero, C.; Jiang, P.; Pach, E.; Borondics, F.; West, M. W.; Tuxen, A.; Chintapalli, M.; Carenco, S.; Guo, J.; Salmeron, M. A Reaction Cell with Sample Laser Heating for in Situ Soft X-Ray Absorption Spectroscopy Studies under Environmental Conditions. *J. Synchrotron Radiat.* **2013**, DOI: 10.1107/S0909049513002434.

(11) Iglesia, E. Design, Synthesis, and Use of Cobalt-Based Fischer−Tropsch Synthesis Catalysts. *Appl. Catal., A* **1997**, *161*, 59−78.

(12) Bezemer, G. L.; Bitter, J. H.; Kuipers, H. P. C. E.; Oosterbeek, H.; Holewijn, J. E.; Xu, X.; Kapteijn, F.; van Dillen, A. J.; de Jong, K. P. Cobalt Particle Size Effects in the Fischer−Tropsch Reaction Studied with Carbon Nanofiber Supported Catalysts. *J. Am. Chem. Soc.* **2006**, *128*, 3956−64.

(13) Herranz, T.; Deng, X.; Cabot, A.; Guo, J.; Salmeron, M. Influence of the Cobalt Particle Size in the CO Hydrogenation Reaction Studied by in Situ X-Ray Absorption Spectroscopy. *J. Phys. Chem. B* **2009**, *113*, 10721−7.

(14) Prieto, G.; Martínez, A.; Concepción, P.; Moreno-Tost, R. Cobalt Particle Size Effects in Fischer−Tropsch Synthesis: Structural and in Situ Spectroscopic Characterization on Reverse Micelle-Synthesized Co/ITQ-2 Model Catalysts. *J. Catal.* **2009**, *266*, 129−144.

(15) Iablokov, V.; Beaumont, S. K.; Alayoglu, S.; Pushkarev, V. V; Specht, C.; Gao, J.; Alivisatos, A. P.; Kruse, N.; Somorjai, G. A. Size-Controlled Model Co Nanoparticle Catalysts for CO_2 Hydrogenation: Synthesis, Characterization, and Catalytic Reactions. *Nano Lett.* **2012**, *12*, 3091−6.

(16) Alonso, D. M.; Wettstein, S. G.; Dumesic, J. A. Bimetallic Catalysts for Upgrading of Biomass to Fuels and Chemicals. *Chem. Soc. Rev.* **2012**, *41*, 8075−8089.

(17) Nørskov, J. K.; Abild-Pedersen, F.; Studt, F.; Bligaard, T. Density Functional Theory in Surface Chemistry and Catalysis. *Proc. Natl. Acad. Sci. U.S.A.* **2011**, *108*, 937−43.

(18) Mouaddib, N.; Perrichon, V.; Martin, G. A. Characterization of Copper-Cobalt Catalysts for Alcohol Synthesis from Syngas. *Appl. Catal., A* **1994**, *118*, 63−72.

(19) Rocha, A. L.; Solórzano, I. G.; Vander Sande, J. B. Heterogeneous and Homogeneous Nanoscale Precipitation in Dilute Cu−Co Alloys. *Mater. Sci. Eng., C* **2007**, *27*, 1215−1221.

(20) Li, G.; Wang, Q.; Li, D.; Lü, X.; He, J. Structure Evolution during the Cooling and Coalesced Cooling Processes of Cu−Co Bimetallic Clusters. *Phys. Lett. A* **2008**, *372*, 6764−6769.

(21) Ahmed, J.; Ganguly, A.; Saha, S.; Gupta, G.; Trinh, P.; Mugweru, A. M.; Lofland, S. E.; Ramanujachary, K. V.; Ganguli, A. K. Enhanced Electrocatalytic Activity of Copper−Cobalt Nanostructures. *J. Phys. Chem. C* **2011**, *115*, 14526−14533.

(22) Chanenchuk, C. A.; Yates, I. C.; Satterfield, C. N. The Fischer−Tropsch Synthesis with a Mechanical Mixture of a Cobalt Catalyst and a Copper-Based Water Gas Shift Catalyst. *Energy Fuels* **1991**, *5*, 847−855.

(23) Subramanian, N. D.; Kumar, C. S. S. R.; Watanabe, K.; Fischer, P.; Tanaka, R.; Spivey, J. J. A DRIFTS Study of CO Adsorption and Hydrogenation on Cu-Based Core−Shell Nanoparticles. *Catal. Sci. Technol.* **2012**, *2*, 621.

(24) Ewers, T. D. Porous Core-Shell Nanostructures for Catalytic Applications. PhD Thesis, University of California Berkeley, Berkeley, CA, 2012.

(25) Bazin, D.; Kovacs, I.; Guczi, L.; Parent, P.; Laffon, C.; De Groot, F.; Ducreux, O.; Lynch, J. Genesis of Co/SiO_2 Catalysts: XAS Study at the Cobalt $L_{III,II}$ Absorption Edges. *J. Catal.* **2000**, *189*, 456−462.

(26) Liu, H.; Yin, Y.; Augustsson, A.; Dong, C.; Nordgren, J.; Chang, C.; Alivisatos, P.; Thornton, G.; Ogletree, D. F.; Requejo, F. G.; et al. Electronic Structure of Cobalt Nanocrystals Suspended in Liquid. *Nano Lett.* **2007**, *7*, 1919−1922.

(27) Tuxen, A.; Carenco, S.; Chintapalli, M.; Chuang, C.-H.; Escudero, C.; Pach, E.; Jiang, P.; Borondics, F.; Beberwyck, B. J.; Alivisatos, A. P.; et al. Size-Dependent Dissociation of Carbon Monoxide on Cobalt Nanoparticles. *J. Am. Chem. Soc.* **2013**, *135*, 2273−2278.

(28) Smith, M. L.; Campos, A.; Spivey, J. J. Reduction Processes in Cu/SiO_2, Co/SiO_2, and $CuCo/SiO_2$ Catalysts. *Catal. Today* **2012**, *182*, 60−66.

(29) de Smit, E.; de Groot, F. M. F.; Blume, R.; Hävecker, M.; Knop-Gericke, A.; Weckhuysen, B. M. The Role of Cu on the Reduction Behavior and Surface Properties of Fe-Based Fischer−Tropsch Catalysts. *Phys. Chem. Chem. Phys.* **2010**, *12*, 667−80.

(30) In AP-XPS conditions, the CO/H_2 ratio was set to 1 to limit the amount of H_2 to be pumped by the turbopumps while recording spectra and to limit gas exposure of the analyzer.

(31) Smith, M. L.; Kumar, N.; Spivey, J. J. CO Adsorption Behavior of Cu/SiO_2, Co/SiO_2, and $CuCo/SiO_2$ Catalysts Studied by in Situ DRIFTS. *J. Phys. Chem. C* **2012**, *116*, 7931−7939.

(32) Domke, M.; Xue, C.; Puschmann, A.; Mandel, T.; Hudson, E.; Shirley, D. A.; Kaindl, G. Carbon and Oxygen K-Edge Photoionization of the CO Molecule. *Chem. Phys. Lett.* **1990**, *173*, 122−128.

(33) Myneni, S.; Luo, Y.; Näslund, L. Å.; Cavalleri, M.; Ojamäe, L.; Ogasawara, H.; Pelmenschikov, A.; Wernet, P.; Väterlein, P.; Heske, C.; et al. Spectroscopic Probing of Local Hydrogen-Bonding Structures in Liquid Water. *J. Phys.: Condens. Matter* **2002**, *14*, L213−L219.

(34) (a) Twigg, M. V.; Spencer, M. S. Deactivation of Supported Copper Metal Catalysts for Hydrogenation Reactions. *Appl. Catal., A* **2001**, *212*, 161−174. (b) Twigg, M.; Spencer, M. Deactivation of Copper Metal Catalysts for Methanol Decomposition, Methanol Steam Reforming and Methanol Synthesis. *Top. Catal.* **2003**, *22*, 191−203. (c) Huang, H.; Wang, S.; Wang, S.; Cao, G. Deactivation Mechanism of Cu/Zn Catalyst Poisoned by Organic Chlorides in Hydrogenation of Fatty Methyl Ester to Fatty Alcohol. *Catal. Lett.* **2009**, *134*, 351−357.

(35) Chaâbane, N.; Lazzari, R.; Jupille, J.; Renaud, G.; Avellar Soares, E. CO-Induced Scavenging of Supported Pt Nanoclusters: A GISAXS Study. *J. Phys. Chem. C* **2012**, *116*, 23362−23370.

(36) Vollmer, S.; Witte, G.; Wöll, C. Determination of Site Specific Adsorption Energies of CO on Copper. *Catal. Lett.* **2001**, *77*, 97−101.

(37) Liao, K.; Fiorin, V.; Gunn, D. S. D.; Jenkins, S. J.; King, D. A. Single-Crystal Adsorption Calorimetry and Density Functional Theory of CO Chemisorption on fcc Co{110}. *Phys. Chem. Chem. Phys.* **2013**, *15*, 4059−4065.

(38) Wu, G.; Li, Y.-W.; Xiang, H.-W.; Xu, Y.-Y.; Sun, Y.-H.; Jiao, H. Density Functional Investigation on Copper Carbonyl Complexes. *J. Mol. Struct.: THEOCHEM* **2003**, *637*, 101−107.
(39) Frankenburg, W. G. *Advances in Catalysis and Related Subjects*; Academic Press: Waltham, MA, 1952; Vol. *4*, p 403.
(40) Detection of gas-phase $Co_2(CO)_8$ is challenging considering the tiny amounts involved in this study and because it deposits back on any cold surface.
(41) Wender, I.; Sternberg, H. W.; Friedel, R. A.; Metlin, S. J.; Markby, R. E. *The Chemistry and Catalytic Properties of Cobalt and Iron Carbonyls*; U.S. Government Printing Office: Washington, DC, 1962; Section 2, pp 3 and 15.
(42) Cardner, P. J.; Gartner, A.; Cunninghame, R. G.; Robinson, B. H. Bond Energies in Dicobalt Octacarbonyl and Bromo- and Chloro-Methylidynetricobalt Enneacarbonyls. *J. Chem. Soc., Dalton Trans.* **1975**, 2582.